Contents lists available at ScienceDirect

Heliyon

Research article

ADDISC lumbar disc prosthesis: Analytical and FEA testing of novel implants

Amparo Vanaclocha [a], Vicente Vanaclocha [b,*], Carlos M. Atienza [c,d], Pablo Jorda-Gomez [e], Cristina Diaz-Jimenez [f], Jose A. Garcia-Lorente [g], Nieves Saiz-Sapena [h], Leyre Vanaclocha [i]

[a] *Escuela de Doctorado, Universitat Politècnica de Valencia, Camí de Vera, s/n, 46022, Valencia, Spain*
[b] *University of Valencia, Avenida de Blasco Ibáñez, 15, 46010 Valencia, Spain*
[c] *Instituto de Biomecánica (IBV), Universitat Politècnica de Valencia, Camí de Vera, s/n, 46022 Valencia, Spain*
[d] *Instituto de Biomecánica de Valencia-CIBER BBN, Grupo de Tecnología Sanitaria (GTS-IBV), Camí de Vera, s/n, 46022 Valencia, Spain*
[e] *Hospital General Universitario de Castellón, Avenida de Benicàssim, 128, 12004 Castelló de la Plana, Spain*
[f] *Industry Association of Navarra, Carretera de Pamplona, 1, 31191 Cordovilla, Navarra, Spain*
[g] *Public University of Navarra, Av. Cataluña, s/n, 31006 Pamplona, Spain*
[h] *Hospital General Universitario de Valencia, Avenida Tres Cruces 2, Valencia, Spain*
[i] *Medius Klinik, Ostfildern-Ruit Klinik für Urologie, Hedelfinger Strasse 166, 73760 Ostfildern, Esslingen, Baden-Wurtemberg, Germany*

ARTICLE INFO

ABSTRACT

The intact intervertebral disc is a six-freedom degree elastic deformation structure with shock absorption. "Ball-and-socket" TDR do not reproduce these properties inducing zygapophyseal joint overload. Elastomeric TDRs reproduce better normal disc kinematics, but repeated core deformation causes its degeneration. We aimed to create a new TDR (ADDISC) reproducing healthy disc features. We designed TDR, analyzed (Finite Element Analysis), and measured every 500,000 cycles for 10 million cycles of the flexion-extension, lateral bending, and axial rotation cyclic compression bench-testing. In the inlay case, we weighted it and measured its deformation.

ADDISC has two semi-spherical articular surfaces, one rotation centre for flexion, another for extension, the third for lateral bending, and a polycarbonate urethane inlay providing shock absorption. The first contact is between PCU and metal surfaces. There is no metal-metal contact up to 2000 N, and CoCr28Mo6 absorbs the load. After 10 million cycles at 1.2–2.0 kN loads, wear 140.96 mg (35.50 mm^3), but no implant failures. Our TDR has a physiological motion range due to its articular surfaces' shape and the PCU inlay bumpers, minimizing the facet joint overload. ADDISC mimics healthy disc biomechanics and Instantaneous Rotation Center, absorbs shock, reduces wear, and has excellent long-term endurance.

1. Introduction

Lumbar fusion, the gold standard for degenerative disc disease [1], disturbs the spine's biomechanics. Motion-sparing techniques aim to prevent its long-term consequences. Although preliminary results with Total Disc Replacement (TDR) seemed promising, long-term problems arose [2] attributed to a lack of spinal biomechanics reproduction [3] and excessive motion range [3].

---

* Corresponding author.
E-mail address: vivava@uv.es (V. Vanaclocha).

The intervertebral disc is not a diarthrodial joint but an elastic block with a shock-absorbing capacity [4], load cushioning [5], weight dispersion [5], and a movable Instantaneous Center of Rotation (ICR) [6]. Elastomeric TDRs aimed to reproduce these features [7,8], but repetitive deformation has induced long-term degeneration with cracks and even extrusion [9].

We designed the ADDISC™ (Advanced Disc Design In Spinal Concepts) (Socinser, Gijon, Spain) to reproduce the intact spine's biomechanics and ICR, with shock absorption capacity and the lowest possible wear rate for a ball-and-socket (BaS) TDR.

This publication aims to report our new complete lumbar disc replacement, explaining its properties and characteristics. We will also emphasize its advantages over other TDRs available in the market.

2. Materials and methods

A previous study on cadaveric lumbar spines determined the intervertebral disc ICR and the articular geometric profiles that reproduce its biomechanics [10].

We did a TDR 3D computerized design, validated it, found mobility ranges and ICR, and submitted the prototypes to laboratory fatigue and wear tests. Then, with the SOLIDWORKS 2019 (Dassault Systems, Vélizy, Villacublay Cedex, France), we designed the articular surfaces focusing on a mobile axis strategy with the data from our previous study [10]. The constructive solution was a cylindrical surface for flexion-extension and a revolution one for lateral bending and axial rotation.

We designed all components to withstand the physiological loads specified in the ASTM F 2077-03 standard and the prosthesis external geometry defined with the vertebral bodies' anthropometric data [10].

We determined two areas (z1 and z2) that were overloaded. Next, we performed stress calculations to ascertain whether the implant would fail under physiological or long-time repetitive loading with an FEA (Finite Element Analysis). Finally, we calculated the stress values with the following equations (units in parenthesis, numbered 1, 2 and 3):

- Inertia (Eq. (1))

$$I = \frac{\pi(2r)^4}{64} \tag{1}$$

where: I = Inertia (m^4) and r = Radius of rod and implant's core (m), m = metres.

- Flexor-extensor bending moment (Eq. (2))

$$M = dF \tag{2}$$

where: M = Flexor-extensor bending moment (Nm), d = Length of the implant's core portion (m) and F = Force (N), N = Newtons, Nm = Newtons meter.

- Stress (Eq. (3))

$$\sigma = \frac{F}{A} \pm \left(\frac{M}{I}\right) r \tag{3}$$

where: σ = Stress (N/m^2), F = Force (N), A = Area (m^2), M = Flexor-extensor bending moment (Nm) and I = Inertia (m^4).

2.1. TDR design validation with a FEA (Finite Element Analysis)

We did it with the ANSYS Workbench Student 14.5 software (Ansys Inc., Canonsburg, Pennsylvania, USA) FEA, following the ASTM F1717 – 18. In addition, we considered the worst possible scenario, including the implant's bone/soft tissue interactions. After importing the geometry into ANSYS, we generated a mesh and adjusted it to resolve the geometry satisfactorily. Finally, the standard gradient analysis indicated that the model could be valid.

We carried the following FEA:

1 Compression (2000 N), the maximum reported load for the intact normal human lumbar spine [11].
2 Lateral bending (7.5 Nm) [12].
3 Compression (2000 N) combined with lateral bending (7.5 Nm).
4 Flexion (7.5 Nm).
5 Extension (7.5 Nm).
6 Flexion (7.5 Nm) combined with compression (2000 N).
7 Extension (7.5 Nm) combined with compression (2000 N).

The load distribution complied with the ASTM F1717 – 1813, applying the force on the upper CoCr28Mo6 piece. In addition, we used two restrictions on the model:

- Fixed support (blue color in Figure S1S, supplementary material).
- Displacement (restriction on z-axis – height).

Figure S1Sa (Supplementary Material) shows the FEA model PCU inlay restrictions. Figures S1Sb, S1Sc, S1Sd (Supplementary Material) show where we applied forces and moments.

We measured the ADDISC TDR range of motion (ROM) with the SOLID WORKS design program. The mobility range depends on the geometry of the articular surfaces and the PCU inlay elastic deformation.

2.2. Low carbon CoCr28Mo6 alloy validation

We did it following the ASTM F-1537 ISO 5832:12, including wear and friction tests against a CoCr28Mo6 ball, corrosion resistance in bovine serum (BS), and ion release after wear studies.

For the wear test, we employed the Microtest MT/30/NI (Microtest, Madrid, Spain) equipment using a ball-on-disk configuration and BS containing 23 g/l of proteins at 7.0 pH and 37 ± 0.2 °C. We evaluated the samples against a CoCr28Mo6 alloy ball with a 12.7 mm diameter, 15 nm Ra, and 30 Hardness Rockwell C. We measured the wear tracks' size with an optical profilometer and calculated the wear rate from the volume loss.

Corrosion tests followed the ASTM G5-94 standard, cleaning the specimens with ethanol beforehand. We performed the electrochemical studies using a Gamry Reference 600 potentiostat (Gamry, PA, USA) in Hank's Balanced Salt Solution (pH 6.8) at 37.2 ± 0.2 °C. The corrosion cell had an Ag/AgCl reference electrode, a Pt counter electrode, and the sample as the working electrode. We recorded for 15 min the free corrosion potential (E0C) and then the potentiodynamic polarization with a scan ranging from E0C-1.5 V to E0C + 1.5 V and a 0.16 mV/s rate. Next, we determined the corrosion rate using the polarization curve's Tafel slope.

With the BS used during each wear test we did the alloy ion releasing test. We divided into ten 30 ml samples and analyzed them by inductively coupled plasma mass spectrometry (ICP-MS) using Agilent 7500ce (Santa Clara, CA, USA), registering the Cobalt, Chromium, and Molybdenum metal ions released. Following the data published in the literature, we considered the TDR mechanical and wear tests a complete fatigue test.

2.3. Low carbon CoCr28Mo6 alloy wear

We used the Institute of Biomechanics of Valencia spine wear stimulator, complying with ISO 18192-1 standard [14] (Figure S2S, supplementary material). This machine has basins to submerge the TDR samples during the test in a BS solution with a protein content similar to the human synovial fluid [15,16], penicillin, amphotericin, and EDTA and kept at 37 ± 2 °C.

We subjected the implants to variable compression forces and different relative angular displacements, representing normal loading conditions for the intervertebral discs.

The prosthesis components underwent gravimetric evaluation following the ISO 18192-1:2008, ISO 18192-2:2010, and ISO 14242-2 standards. We evaluated five TDR samples for 10 million cycles at 1 Hz frequency cyclic compression combined with 3D motion in flexion-extension, lateral bending, and axial rotation, simulating a ten-year TDR use (Figure S3S, supplementary material). Additionally, five control implants underwent the same loadings but without motion to measure the PCU inlay weight changes due to water absorption.

We measured the TDRs' weight every 500,000 cycles. Given the ability of the PCU inlay to hydrate, the worn material was the TDR weight loss and increased weight due to PCU fluid absorption. Before weighing, we thoroughly cleaned the samples from particles that might confound the results and the washings collected to analyze wear debris and particle characterization. In addition, we measured medial-lateral, anterior-posterior, and height PCU inlay changes at 500,000 cycle intervals controlling its deformation.

3. Statistical analysis

We analyzed the data with Excel (Microsoft Corporation, Redmond, WA, USA) and SPSS 26 (IBM Corporation, Armonk, New York, US). We calculated the movement's angles and parameters with the GNU Octave software (https://www.gnu.org/software/octave/index). Finally, we combined the statistical analysis R (R Development Core Team) [17,18] with the Deducer user interface (I. Fellows, "Deducer: A Data Analysis GUI for R", Journal of Statistical Software, vol. 49, No. 8, 2012).

4. Results

4.1. ADDISC TDR 3D computerized design

We designed the articular surfaces with the results from a previous lumbar spine kinematic study [26].

The articular areas were a cylindrical surface for the flexion-extension and a revolution for the lateral bending and axial rotation (Fig. 1A and C). In addition, it had two distinctive semi-spherical areas, one for flexion and another for extension (Fig. 1B). Thus, there are two rotation centres for flexion-extension and a third for lateral bending, each with a 2.5 mm radius (Fig. 1A–C).

The design had two fixed rotation axes, one for flexion-extension and another for lateral bending, the first in the midline 17 mm below the articular surface of the lower prosthesis component and the second 1.3 mm above the articular surface of the upper metallic piece in the sagittal plane. We show the ADDISC artistic rendition of the whole implant and its components in Fig. 2A and B superior

piece, 2C and 2D PCU inlay, and 2E and 2F inferior part. In addition, we see the front (2G), above or below (2H), and back view (2I) of our TDR once mounted.

The ideal TDR biomaterial should be biocompatible. It should also have a Young elastic modulus like the vertebral endplate bone, high tensile and fatigue strengths and stiffness, and that generates no artefacts on radiological imaging.

In the intact spine, the Young elastic modulus is 1.66 MPa for the nucleus pulposus, 12.99 MPa for the annulus, 3.87 MPa for the cancellous bone, and 14.64 MPa for the cortical bone [19]. Furthermore, the Poisson ratio is 0.40 for the nucleus pulposus and 0.35 for the annulus [19], and the intact disc stands loads between 800 and 3000 N [20,21]. Accordingly, our TDR should have an elastic modulus similar to the cortical vertebral body bone (14.64 MPa) (under heavy loads, the bone collapses before the intervertebral disc), a Poisson ratio of 0.40, and stand a minimum 3000 N load.

We selected the CoCr28Mo6 alloy for the top and bottom components, with a 240 GPa Young elastic modulus [22,23], a 0.30 Poisson's ratio, and a 15.7 GPa nanoindentation [24].

We introduced an intermediate piece to limit excessive movement and provide shock absorption (Fig. 1A–C). It has a ring-shaped design with lateral rows that adjust to slightly longer cavities in the metallic endplates to limit the movement range in axial rotation (Fig. 1C). For the inlay, we selected a PCU, Bionate 80A (DSM Biomedical, California, USA) [25]. Its elastic modulus is 22 MPa (vertebral body cortical bone 14.64 MPa) 19 and a 0.49 Poisson ratio [25] (nucleus pulposus 0.40).

With a 2000 N force, the maximum PCU inlay deformation was 461 μm (x-axis), 385 μm (y-axis), and 466 μm (z-axis). The distance between the metallic plates is 2.75 mm, and the PCU thickness is 3.30 mm. Therefore, the PCU deformation must be 0.55 mm in the z-axis before the metallic articular surfaces come in contact, and this does not happen up to 2000 N loads.

4.2. CoCr28Mo6 allow wear

The dominant wear mode was adhesive with only minor deposition at the wear track edge, with a 0.26 ± 0.01 friction coefficient and a $7.20 \pm 0.77) \times 10^{-4}$ m^3/Nm average wear rate. However, the wear mark was abrasive, and the particles detached from the surface remained accumulated on the edges, contributing to the depth of the wear groove (Figure S4S, supplementary material). After wear tests, we analyzed the BS used as a medium fluid by inductively coupled plasma mass spectrometry, showing a low-weight ion release ratio of CoCr28Mo6 alloy (approximately 1000 ppb).

4.3. CoCr28Mo6 alloy corrosion

Evaluating polarization (Figure S5S supplementary material) and Tafel curves, we saw a 10^{-7} A/cm^2 current density and a corrosion potential of 300 mV and $1,7 \times 10^{-3}$ mm/year.

4.4. ADDISC TDR FEA analysis

The results we got in the range of motion (ROM) with the Solid Works design program and under a 2000 N load were $-3°$ in
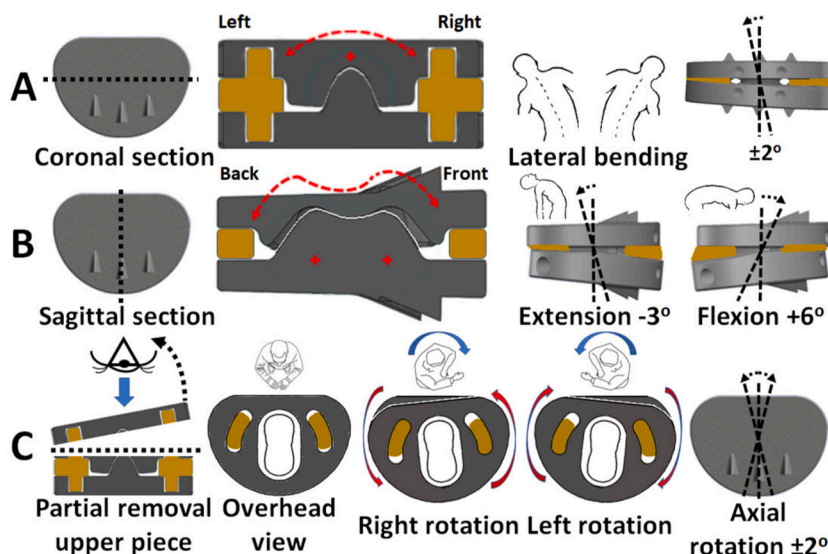
Fig. 1. TDR articular surfaces shape. (A) View from the front of the coronal section. (B) View from the side after the sagittal section. (C) View from above. The radius of the articular surfaces is 2.50 mm. Next, we depict the PCU inlay in brown color. The two top rows show the articular surfaces, and we see that their shapes and the PCU inlay deformation control excess mobility. Meanwhile, the lower line presents how the PCU intermediate piece bumpers block limits axial rotation's excessive movement.

A. Vanaclocha et al.

Heliyon 9 (2023) e13540
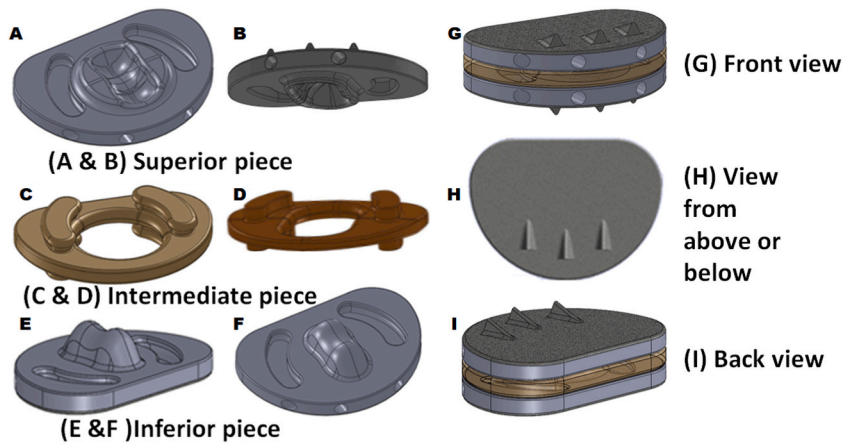
Fig. 2. ADDISC artistic rendition of the whole implant and its components. A and B superior piece, C and D PCU inlay, E and F inferior part. We see the front (G), above or below (H) and back view (I) of the whole ADDISC TDR on the right side.

extension, +6° in flexion, ±2° in lateral bending, and ±2° in axial rotation.

We imported the TDR computerized model into the ANSYS Workbench, complying with the F1717-18 regulation [13]. Next, we generated a mesh using the patch-conforming method and adjusted the mesh to resolve the geometry satisfactorily, utilizing the standard gradient analysis. In addition, the contact between PCU and CoCr28Mo6 components was 'no separation', allowing sliding without spreading. Finally, we analyzed the CoCr28Mo6 and PCU components, considering the most restrictive situation: the smallest configuration. As a result, we observed no regions of atypical stress accumulation, and no von Mises stress value reached the CoCr28Mo6 alloy yield (953.4 ± 132.1 MPa) [23] or fatigue strengths (725 MPa), showing that the implant would resist normal loading conditions (Fig. 3A and B).

4.5. ADDISC laboratory bench studies

We evaluated a total of 12 ADDISC samples. The metallic pieces' most significant stresses arose during flexion combined or not with compression and the weakest during lateral bending. Furthermore, the PCU inlay maximum total deformation occurred during compression combined with flexion, whereas the minimum appeared during lateral bending (Table 1). Finally, the equivalent tensions were significantly lower for PCU than for CoCr28Mo6, as the metallic pieces support the load while the PCU inlay acts as a shock-absorbing mechanism (Table 2, Figure S6S).

The ADDISC TDR prosthesis showed 23.15 ± 1.25 mg and 5.7 ± 0.26 mm^3 wear for the first million cycles, with 140.96 ± 12.35 mg (35.50 ± 3.87 mm^3) accumulated average wear at 10 million cycles (Table 3). We show the evolution of the ADDISC prosthesis's different components' volumetric wear in Fig. 4 (4A for the ADDISC total volumetric wear, 4B for the upper piece, 4C for the inferior component and 4D for the PCU inlay).
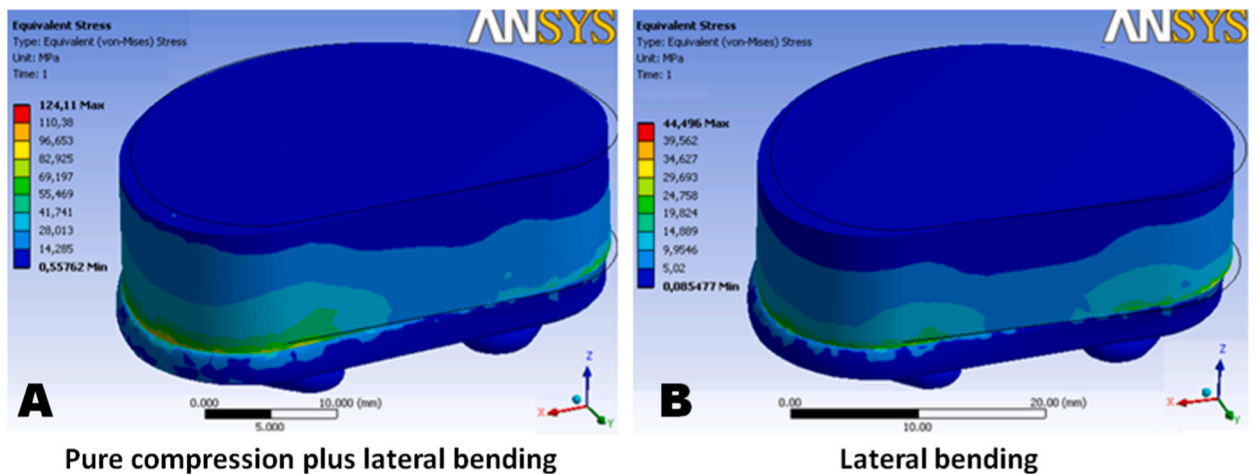
Fig. 3. ANSYS equivalent stress von Mises values of the CoCr28Mo6 and PCU region of the implant's interest in (A) pure compression (2000 N) combined with lateral bending (7.5 N) and (B) lateral bending (7.5 N). The colors are primarily blue, indicating low stress and von Misses values.

Table 1

Results obtained for the different loading patterns applied to the TDR ± standard deviation in pure compression under 2000 N, lateral bending under 7.5 N, pure compression (under 2000 N) plus lateral bending (under 7.5 N), flexion (under 7.5 N), extension (under 7.5 N), pure compression (under 2000 N) plus flexion (7.5 N) and pure compression (under 2000 N) plus extension (7.5 N).

LOADING PATTERN	Equivalent tension (MPa)	PCU tension equivalents (MPa)	Equivalent deformation (mm)	Total deformation (mm)	Deformation x-axis (mm)	Deformation y-axis (mm)	Deformation z-axis (mm)
Pure compression (2000 N)	40.943 ± 5.782	12.396 ± 2.167	0.563 ± 0.034	0.521 ± 0.024	0.493 ± 0.049	0.441 ± 0.048	0.002 ± 0.001
Lateral bending (7.5 Nm)	40.297 ± 4.985	4.856 ± 0.879	0.221 ± 0.027	0.370 ± 0.019	0.251 ± 0.037	0.240 ± 0.021	0.209 ± 0.001
Pure compression (2000 N) + lateral bending (7.5 Nm)	50.775 ± 5.018	17.214 ± 3.472	0.782 ± 0.042	0.778 ± 0.036	0.739 ± 0.021	0.678 ± 0.037	0.003 ± 0.001
Flexion (7.5 Nm)	56.045 ± 4.357	5.686 ± 1.104	0.258 ± 0.025	0.546 ± 0.081	0.375 ± 0.011	0.295 ± 0.042	0.279 ± 0.036
Extension (7.5 Nm)	56.045 ± 4.882	5.686 ± 1.189	0.258 ± 0.023	0.546 ± 0.072	0.373 ± 0.037	0.422 ± 0.031	0.360 ± 0.018
Pure compression (2000 N) + flexion (7.5 Nm)	62.116 ± 5.901	14.074 ± 2.732	0.640 ± 0.035	0.923 ± 0.063	0.709 ± 0.017	0.445 ± 0.086	0.046 ± 0.007
Pure compression (2000 N) + extension (7.5 Nm)	59.169 ± 5.642	15.294 ± 3.017	0.695 ± 0.041	0.770 ± 0.056	0.709 ± 0.071	0.711 ± 0.016	0.020 ± 0.005

During the wear tests, no TDR component broke, suffered damage or cracked. Furthermore, the implant had excellent behavior during 10 million cycles of 1.2 kN and 2.0 kN peak sinusoidal loads.

5. Discussion

The intervertebral disc is an elastic deformation structure, not a diarthrodial joint [5], with six degrees of freedom [7] and shock absorption [26]. Unfortunately, marketed TDRs do not completely reproduce these features, despite improvements in designs, materials, and biomechanics [2], causing long-term problems.

5.1. TDRs and degrees of freedom

BaS TDRs with a UHMWP (ultrahigh molecular weight polyethylene) non-movable inlay (Prodisc-L) have only three, with fixed axial rotation ICR7 overloading facet joints [27,28]. If the inlay moves back-to-front (Activ-L) and sideways (Mobidisc), it has five degrees of freedom [7] but lacks shock absorption. The inlay movement increases the tolerance to minor misplacements. It also creates less bone interface stress [29] but still induces zygapophyseal joint overload [2]. Meanwhile, only the elastomeric TDRs have six degrees of freedom [7,30] and reproduce the intact intervertebral disc features [7]. Our TDR merges BaS and elastomeric designs, providing six degrees of freedom and shock absorption.

5.2. Articulating surfaces geometry

Most BaS TDRs have excessive ROM, particularly in axial rotation [31]. An elliptic shape articular surface restricts motion in axial rotation [32], but no BaS has it. The ADDISC has two semi-spheres reproducing this elliptical shape, limiting axial rotation, controlled further by the C-shaped PCU bumpers.

5.3. ICR and ROM

The intact intervertebral lumbar disc ICR lies in its posterior third and moves with the spine's movements [6,10], 4 mm backward

Table 2

Deformation of PCU inlay made of Bionate 80A (22 MPa. v = 0.49) under different forces and movements, placed between CoCr28Mo6 (241 GPa. v = 0.3) endplates ± standard deviation. Contact mode: No separation. We performed the movements under the loadings mentioned between the brackets.

	COMPONENT	Wear (mg)	Wear (mm^3)
ADDISC	Superior	9.50 ± 4.92	5.55 ± 1.16
	Inferior	9.11 ± 3.72	4.45 ± 1.05
	PCU	23.64 ± 5.67	17.56 ± 3.29
	TOTAL	42.25 ± 12.35	27.12 ± 3.87

Table 3
Accumulated wear during the 10 million cycle test for each ADDISC TDR component ± standard deviation.

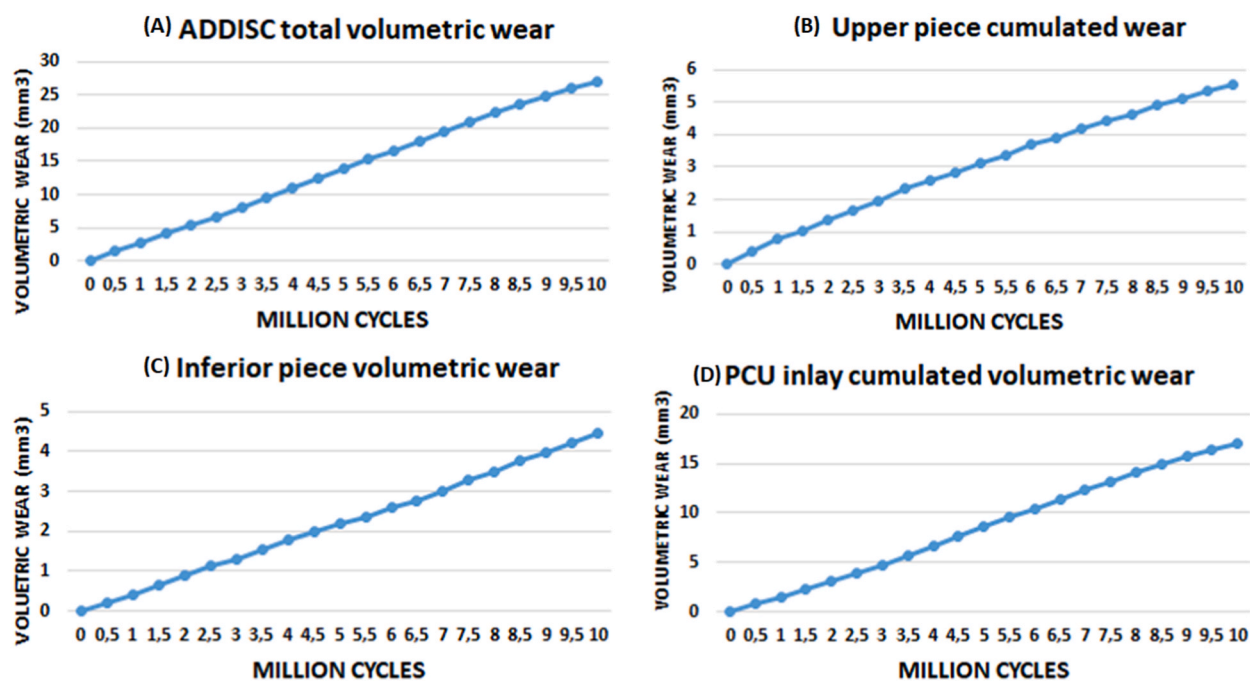| DISC	Author & year	Flexion	Extension	Lateral bending	Axial rotation
Intact disc	Choi 2017	6.7	3.4	3.5	2.2
Charité	Wilke 2012	4	11	9	5
Prodisc-L	Wilke 2012	4	10	9	6
Activ-L	Grupp 2015	8.5	11	8	Not provided
Activ-L	Ha 2009	3.2 ± 0.8 SD	9.0 ± 1.6 SD	9.0 ± 2.2 SD	5.4 ± 0.9 SD
Mobi-C	Hisey 2014	10	10	10	Not provided
Maverick-L	Mathews 2004	5.4	3.41	3.57	2.29
Flexicore	Errico 2005	15	15	15	5
Baguera	Lee 2016	12	12	12	Not provided
Cadisc-L	Mahomed 2012	6	6	10	8
LP-ESP	Lazennec 2013	6	6	2.5	2
M6-L	Patwardhan 2012	13.5 ± 2.3 SD	13.5 ± 2.3 SD	4.5 ± 1.1SD	8.3 ± 1.6 SD
ADDISC		6	3	2	2

Fig. 4. Cumulated wear ± range for the ADDISC TDR (4A for the ADDISC total volumetric wear, 4B for the upper piece, 4C for the inferior component and 4D for the PCU inlay). Again, this wear is low for all ADDISC integrating pieces, more significant for the PCU inlay than metallic articular surfaces.

in extension and 8 mm frontwards in flexion [6]. Intact intervertebral disc ICR reproduction is essential to minimize wear [33] and adverse outcomes [3].

TDRs with ICR at the geometrical disc centre (Prodisc-L [34], Activ-L [35], Flexicore [36]) depend on spine structures to limit excessive motion, particularly in axial rotation [37], inducing zygapophyseal joint damages [38]. TDRs with ICR at the disc posterior third (Maverick-L [39]) create less facet joint overload [39,40]. The elastomeric LP-ESP TDR reproduces ICR better than BaS TDRs [7, 41], but long-term clinical results are pending. We designed ADDISC to mimic intact intervertebral disc ICR, but clinical studies are still lacking.

5.4. Motion range

As muscles, ligaments, and zygapophyseal joints must control TDRs excessive ROM [37], causing chronic low back pain [42], reproducing the physiological ROM is essential [43]. Moreover, published data show the ROM is abnormal for all, not only BaS but also elastomeric TDRs like Cadisc-L [44], ML-6 [37], and even the LP-ESP™ [7]. Meanwhile, ADDISC allows a more physiological ROM in all axes (Table 4).

5.5. Ball radius, motion range and wear rate

As ball radius increases, mobility decreases in flexion, extension, and lateral bending but increases in axial rotation [31]. Conversely, as this radius decreases, the opposite happens, diminishing frictional torque and reproducing better intact intervertebral disc ICR [45]. As a result, manufacturers minimized TDR wear with a <12 mm ball radius diameter [46]. Meanwhile, ADDISC, with a 2.5 mm articulating surface radius, has the lowest published wear rate [39,47–49].

5.6. Zygapophyseal joint overload

Fixed-core TDRs increase it by>10% while mobile-core reduce it by>50% [50], 79% smaller for semi-constrained than non-constrained TDRs6. In flexion, facet joint load is similar to the intact disc for semi-constrained [35] but increases for non-constrained TDRs [51]. In extension, this load increased in all but more in the non-constrained TDRs [35]. Zygapophyseal joint load increased significantly in lateral bending and axial rotation, particularly for non-constrained TDRs [35]. Charitè (non-constrained) increases facet joint load in all movements, particularly lateral bending [28].

5.7. Shock-absorbing capacity

Only elastomeric TDRs have it [7,41], transforming force into deformation, which can cause degradation with cracks or extrusion [9]. It is almost absent in BaS [52]. ADDISC PCU inlay provides shock absorption until the metallic surfaces withstand loads over 2000 N (Table 2, Fig. S6S supplementary material).

5.8. Wear rate and debris generation

Metal-on-polyethylene has more wear than MoM (metal-on-metal) TDRs [47]. The published wear rate in mm^3/million cycles is 19.35 ± 1.16 (Charité), 16.59 ± 0.95 (Prodisc-L), and 2.7 ± 0.3 (Activ-L) [48] for UHMWP TDRs, 1.7 (Freedom) for PCU [53] and 1.3 ± 0.6 (Maverick-L) [39,49] for MoM but ADDISC has the lowest (1.1 ± 0.1) (Fig. 5).

Even though the long-term impact of metal wear debris from MoM TDRs is still unclear [54], some cases are reported [55], which could be an issue for the ADDISC in the long run.

6. Strengths

We based the ADDISC design on a previous lumbar spine biomechanical study conducted with kinematic analysis techniques. In addition, we incorporated characteristics to avoid zygapophyseal joint overload adjacent level disease, minimize wear, osteolysis, loosening, and subsidence.

7. Limitations

The number of samples evaluated is limited. We must continue the tests for 30 million cycles to assess long-term results.

8. Conclusions

ADDISC reproduces the ISO standard requirements, mimics intact disc biomechanics and ICR, avoids BaS TDR's excess movement range, minimizes zygapophyseal joint load, and reduces wear. ADDISC has good endurance under dynamic loading conditions and excellent response to axial compression loading without long-term failure. In addition, PCU inlay is shock-absorbing and does not crack under five times physiological loads. ADDISC has better wear rates than other TDRs.

Author contribution statement

Amparo Vanaclocha, Vicente Vanaclocha: Conceived and designed the experiments; Performed the experiments; Wrote the paper.

Carlos M. Atienza: Conceived and designed the experiments; Performed the experiments; Contributed reagents, materials, analysis tools or data; Wrote the paper.

Pablo Jordá-Gómez: Performed the experiments. Analyzed and interpreted the data.

Cristina Diaz-Jimenez, Jose A. Garcia-Lorente: Performed the experiments, Analyzed and interpreted the data, Contributed reagents, materials, analysis tools or data.

Nieves Saiz-Sapena: Performed the experiments, Analyzed and interpreted the data, Wrote the paper.

Leyre Vanaclocha: Performed the experiments, Analyzed and interpreted the data. Contributed reagents, materials, analysis tools or data. Wrote the paper.

Table 4

L_4-L_5 range of motion in degrees for the intact lumbar disc and the different TDRs available. Please note that the manufacturer/research group does not supply data for all TDR movement ranges, especially axial rotation. Remarkably, the movement in the axial rotation is the one that most damages the zygapophyseal joints, and thus, these data would be essential to know them. Also, four TDRs exceed the physiological movement ranges for the intact lumbar disc in flexo-extension.

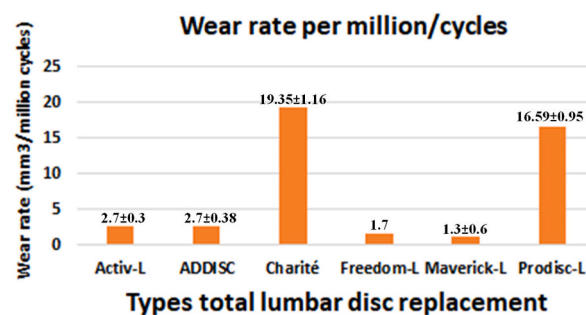| DISC	Author & year	Flexion	Extension	Lateral bending	Axial rotation
Intact disc	Choi 2017	6.7	3.4	3.5	2.2
Charité	Wilke 2012	4	11	9	5
Prodisc-L	Wilke 2012	4	10	9	6
Activ-L	Grupp 2015	8.5	11	8	Not provided
Activ-L	Ha 2009	3.2 ± 0.8 SD	9.0 ± 1.6 SD	9.0 ± 2.2 SD	5.4 ± 0.9 SD
Mobi-C	Hisey 2014	10	10	10	Not provided
Maverick-L	Mathews 2004	5.4	3.41	3.57	2.29
Flexicore	Errico 2005	15	15	15	5
Baguera	Lee 2016	12	12	12	Not provided
Cadisc-L	Mahomed 2012	6	6	10	8
LP-ESP	Lazennec 2013	6	6	2.5	2
M6-L	Patwardhan 2012	13.5 ± 2.3 SD	13.5 ± 2.3 SD	4.5 ± 1.1SD	8.3 ± 1.6 SD
ADDISC		6	3	2	2

Fig. 5. Wear rates (mm^3/1 million cycles) different TDRs with reported data in the literature. It is more significant for Charité and Prodisc-L, lower for Activ-L than Freedom-L and Maverick-L, but minimal for ADDISC.

Data availability statement

The authors do not have permission to share data.

Declaration of interest's statement

The authors declare that they have no known competing financial interests or personal relationships that could have appeared to influence the work reported in this paper.

Appendix A. Supplementary data

Supplementary data to this article can be found online at https://doi.org/10.1016/j.heliyon.2023.e13540.

References

[1] J.Y. Kim, D.S. Ryu, H.K. Paik, et al., Paraspinal muscle, facet joint, and disc problems: risk factors for adjacent segment degeneration after lumbar fusion, Spine J. Off. J. North Am. Spine Soc. 16 (7) (2016) 867–875.

[2] H. Schmidt, S. Midderhoff, K. Adkins, et al., The effect of different design concepts in lumbar total disc arthroplasty on the range of motion, facet joint forces and instantaneous center of rotation of a L4-5 segment, Eur. Spine J. 18 (11) (2009) 1695–1705.

[3] H. Schmidt, F. Galbusera, A. Rohlmann, et al., Effect of multilevel lumbar disc arthroplasty on spine kinematics and facet joint loads in flexion and extension: a finite element analysis, Eur. Spine J. 21 (Suppl 5) (2012) S663–S674.

[4] G. Brzuszkiewicz-Kuźmicka, J. Szczegielniak, D. Bączkowicz, Age-related changes in shock absorption capacity of the human spinal column, Clin. Interv. Aging 13 (2018) 987–993.

[5] M.D. Humzah, R.W. Soames, Human intervertebral disc: structure and function, Anat. Rec. 220 (4) (1988) 337–356.

[6] H. Schmidt, F. Heuer, L. Claes, et al., The relation between the instantaneous center of rotation and facet joint forces – a finite element analysis, Clin. Biomech. 23 (3) (2008) 270–278.

[7] J.-Y. Lazennec, A. Aaron, A. Brusson, et al., The LP-ESP® lumbar disc prosthesis with 6 degrees of freedom: development and 7 years of clinical experience, Eur. J. Orthop. Surg. Traumatol. Orthop. Traumatol. 23 (2) (2013) 131–143.

[8] R. Vicars, R. Hall, P.J. Hyde, Total intervertebral disc prostheses, Compr. Biomater. II 7 (14) (2017) 246–264.

[9] L. Grassner, A. Grillhösl, M. Bierschneider, et al., Disc herniation caused by a viscoelastic nucleus after total lumbar disc replacement-a case report, J. Spine Surg. Hong Kong 4 (2) (2018) 478–482.

[10] A. Vanaclocha-Saiz, C.M. Atienza, V. Vanaclocha, et al., ICR in human cadaveric specimens: an essential parameter to consider in a new lumbar disc prosthesis design, North Am. Spine Soc. J. NASSJ 2 (2020), 100016, https://doi.org/10.1016/j.xnsj.2020.100016.

[11] A.A. White, M.M. Panjabi, Clinical Biomechanics of the Spine, second ed., Lippincott, Philadelphia, 1990, pp. 722–736.

[12] H.J. Wilke, K. Wenger, L. Claes, Testing criteria for spinal implants: recommendations for the standardization of in vitro stability testing of spinal implants, Eur. Spine J. 7 (2) (1998) 148–154.

[13] F04 Committee, Test methods for spinal implant constructs in a vertebrectomy model internet, ASTM International; cited 29th December 2019. Available at: http://www.astm.org/cgi-bin/resolver.cgi?F1717-18.

[14] Norm, ISO 18192-1:2008 internet. ISO, Cited 8th January 2021. Available at: https://www.iso.org/cms/render/live/en/sites/isoorg/contents/data/standard/03/86/38602.html.

[15] P. Moghadas, A. Mahomed, D.W.L. Hukins, et al., Effect of lubricants on friction in laboratory tests of a total disc replacement device, Proc. Inst. Mech. Eng. H 227 (9) (2013) 988–993.

[16] P.J. Hyde, J. Fisher, R.M. Hall, Wear simulation of a polyethylene-on-metal cervical total disc replacement under different concentrations of bovine serum lubricant, Proc. Inst. Mech. Eng. H 230 (5) (2016) 481–488.

[17] K.N. Kirby, D. Gerlanc, BootES: an R package for bootstrap confidence intervals on effect sizes, Behav. Res. Methods 45 (4) (2013) 905–927.

[18] R: the R project for statistical computing internet, Cited 1st April 2016. Available at: https://www.r-project.org/.

[19] Y. Wang, X.-D. Yi, C.-D. Li, The influence of artificial nucleus pulposus replacement on stress distribution in the cartilaginous endplate in a 3-dimensional finite element model of the lumbar intervertebral disc, Medicine 96 (50) (2017), e9149, https://doi.org/10.1097/MD.0000000000009149.

[20] B.A. Frost, S. Camarero-Espinosa, E.J. Foster, Materials for the spine: anatomy, problems, and solutions, Materials 12 (2) (2019) 253, https://doi.org/10.3390/ma12020253.

[21] M. Mills, N. Sarigul-Klijn, Validation of an in vivo medical image-based Young human lumbar spine finite element model, J. Biomech. Eng. (2018), https://doi.org/10.1115/1.4042183.

[22] CarTech® micro-melt® BioDur® CCM® alloy carpenter technology corporation internet, Cited 5th August 2021. Available at: https://metals.ulprospector.com/es/datasheet/e215879/cartech-micro-melt-biodur-ccm-alloy.

[23] E. Bramanti, G. Cervino, F. Lauritano, et al., FEM and Von Mises analysis on prosthetic crowns structural elements: evaluation of different applied materials, Sci. World J. (2017), 1029574, https://doi.org/10.1155/2017/1029574.

[24] Y. Liao, R. Pourzal, P. Stemmer, et al., New insights into hard phases of CoCrMo metal-on-metal hip replacements, J. Mech. Behav. Biomed. Mater. 12 (2012) 39–49.

[25] N. Nic An Ghaill, E.G. Little, Determination of the mechanical properties of Bionate 80A and Bionate 75D for the stress analysis of cushion form bearings, Proc. Inst. Mech. Eng. H 222 (5) (2008) 683–694.

[26] J.F. DeLucca, D. Amin, J.M. Peloquin, et al., Off-axis response due to mechanical coupling across all six degrees of freedom in the human disc, JOR Spine 2 (1) (2019), e1047, https://doi.org/10.1002/jsp2.1047.

[27] Q. Yao, J.C. Wang, A.N. Shamie, et al., The effects of a semiconstrained integrated artificial disc on zygapophyseal joint pressure and displacement, Spine 39 (25) (2014) E1510–E1517.

[28] M.-A. Rousseau, D.S. Bradford, R. Bertagnoli, et al., Disc arthroplasty design influences intervertebral kinematics and facet forces, Spine J. 6 (3) (2006) 258–266.

[29] R.C. Huang, F.P. Girardi, F.P. Cammisa, et al., The implications of constraint in lumbar total disc replacement, J. Spinal Disord. Tech. 16 (4) (2003) 412–417.

[30] C. Schätz, K. Ritter-Lang, L. Gössel, et al., Comparison of single-level and multiple-level outcomes of total disc arthroplasty: 24-month results, Int. J. Spine Surg. 9 (2015) 14, https://doi.org/10.14444/2014.

[31] J. Choi, D.-A. Shin, S. Kim, Biomechanical effects of the geometry of ball-and-socket artificial disc on lumbar spine: a finite element study, Spine 42 (6) (2017) E332–E339.

[32] H.-W. Wei, Y.-F. Chiang, Y.-W. Chen, et al., The effects of different articulate curvature of artificial disc on loading distribution, J. Appl. Biomater. Funct. Mater. 10 (2) (2012) 107–112.

[33] S.M. Kurtz, A. Patwardhan, D. MacDonald, et al., What is the correlation of in vivo wear and damage patterns with in vitro TDR motion response? Spine 33 (5) (2008) 481–489.

[34] J.J. Rawlinson, K.P. Punga, K.L. Gunsallus, et al., Wear simulation of the ProDisc-L disc replacement using adaptive finite element analysis, J. Neurosurg. Spine 7 (2) (2007) 165–173.

[35] S.-K. Ha, S.-H. Kim, D.H. Kim, et al., Biomechanical study of lumbar spinal arthroplasty with a semi-constrained artificial disc (activ L) in the human cadaveric spine, J. Korean Neurosurg. Soc. 45 (3) (2009) 169–175.

[36] A. Valdevit, T.J. Errico, Design and evaluation of the FlexiCore metal-on-metal intervertebral disc prosthesis, Spine J. 4 (6 Suppl) (2004) 276S–288S.

[37] A.G. Patwardhan, R.M. Havey, N.D. Wharton, et al., Asymmetric motion distribution between components of a mobile-core lumbar disc prosthesis: an explanation of unequal wear distribution in CHARITÉ polyethylene cores, J. Bone Joint Surg. Am. 94 (9) (2012) 846–854.

[38] C.S. Shim, S.-H. Lee, H.-D. Shin, et al., CHARITE versus ProDisc: a comparative study of a minimum 3-year follow-up, Spine 32 (9) (2007) 1012–1018.

[39] H.H. Mathews, J.-C. Lehuec, T. Friesem, et al., Design rationale and biomechanics of Maverick Total Disc arthroplasty with early clinical results, Spine J. 4 (6 Suppl) (2004) 268S–275S.

[40] J.-C. Le Huec, Y. Basso, S. Aunoble, et al., Influence of facet and posterior muscle degeneration on clinical results of lumbar total disc replacement: two-year follow-up, J. Spinal Disord. Tech. 18 (3) (2005) 219–223.

[41] D. McNally, J. Naylor, S. Johnson, An in vitro biomechanical comparison of Cadisc™-L with natural lumbar discs in axial compression and sagittal flexion, Eur. Spine J. 21 (Suppl 5) (2012) S612–S617.

[42] A. van Ooij, F.C. Oner, A.J. Verbout, Complications of artificial disc replacement: a report of 27 patients with the SB Charité disc, J. Spinal Disord. Tech. 16 (4) (2003) 369–383.

[43] H.-J. Wilke, R. Schmidt, M. Richter, et al., The role of prosthesis design on segmental biomechanics: semi-constrained versus unconstrained prostheses and anterior versus posterior centre of rotation, Eur. Spine J. 21 (Suppl 5) (2012) S577–S584.

[44] A. Mahomed, P.M. Moghadas, D.E.T. Shepherd, et al., Effect of axial load on the flexural properties of an elastomeric total disc replacement, Spine 37 (15) (2012) E908–E912.

[45] A. Rohlmann, A. Mann, T. Zander, et al., Effect of an artificial disc on lumbar spine biomechanics: a probabilistic finite element study, Eur. Spine J. 18 (1) (2009) 89–97.

[46] P.M. Moghadas, D.E.T. Shepherd, D.W.L. Hukins, et al., Polymer-on-metal or metal-on-polymer total disc arthroplasty: does it make a difference? Spine 37 (21) (2012) 1834–1838.

[47] S.Y. Veruva, M.J. Steinbeck, J. Toth, et al., Which design and biomaterial factors affect clinical wear performance of total disc replacements? A systematic review, Clin. Orthop. 472 (12) (2014) 3759–3769.

[48] T.M. Grupp, J.J. Yue, R. Garcia, et al., Biotribological evaluation of artificial disc arthroplasty devices: influence of loading and kinematic patterns during in vitro wear simulation, Eur. Spine J. 18 (1) (2009) 98–108.

[49] P.E. Paré, F.W. Chan, M.L. Powell, Wear characteristics of the A-MAV™ anterior motion replacement using a spine wear simulator, Wear 263 (2007) 1055–1059.

[50] M. Moumene, F.H. Geisler, Comparison of biomechanical function at ideal and varied surgical placement for two lumbar artificial disc implant designs: mobile-core versus fixed-core, Spine 32 (17) (2007) 1840–1851.

[51] S.-N. Zheng, Q.-Q. Yao, L.-M. Wang, et al., Biomechanical effects of semi-constrained integrated artificial discs on zygapophysial joints of implanted lumbar segments, Exp. Ther. Med. 6 (6) (2013) 1423–1430.

[52] J.C. LeHuec, T. Kiaer, T. Friesem, et al., Shock absorption in lumbar disc prosthesis: a preliminary mechanical study, J. Spinal Disord. Tech. 16 (4) (2003) 346–351.

[53] B. Rischke, R.S. Ross, B.A. Jollenbeck, et al., Preclinical and clinical experience with a viscoelastic total disc replacement, SAS J. 5 (4) (2011) 97–107.

[54] P. Bisseling, D.J. Zeilstra, A.M. Hol, et al., Metal ion levels in patients with a lumbar metal-on-metal total disc replacement: should we be concerned? J. Bone Joint Surg. Br. 93 (7) (2011) 949–954.

[55] R.D. Guyer, J. Shellock, B. MacLennan, et al., Early failure of metal-on-metal artificial disc prostheses associated with lymphocytic reaction: diagnosis and treatment experience in four cases, Spine 36 (7) (2011) E492–E497.